ENVIRONMENTAL RESEARCH
LETTERS

LETTER • **OPEN ACCESS**

Contrasting trends in short-lived and long-lived mesoscale eddies in the Southern Ocean since the 1990s

To cite this article: Fei Shi *et al* 2023 *Environ. Res. Lett.* **18** 034042

ENVIRONMENTAL RESEARCH
LETTERS

LETTER

Contrasting trends in short-lived and long-lived mesoscale eddies in the Southern Ocean since the 1990s

Fei Shi[1], **Yiyong Luo**[2], **Renhao Wu**[1,*], **Qinghua Yang**[1], **Ruiyi Chen**[2], **Chuanyin Wang**[1], **Yichen Lin**[1] and **Dake Chen**[1]

[1] School of Atmospheric Sciences, Sun Yat-sen University, and Southern Marine Science and Engineering Guangdong Laboratory (Zhuhai), Zhuhai, People's Republic of China
[2] Frontier Science Center for Deep Ocean Multispheres and Earth System (FDOMES), Physical Oceanography Laboratory, and College of Oceanic and Atmospheric Sciences, Ocean University of China, 266100 Qingdao, People's Republic of China
* Author to whom any correspondence should be addressed.

E-mail: wurenhao@mail.sysu.edu.cn

Keywords: Southern Ocean, mesoscale eddies, climate change, trends

Supplementary material for this article is available online

OPEN ACCESS

RECEIVED
13 December 2022

REVISED
19 February 2023

ACCEPTED FOR PUBLICATION
27 February 2023

PUBLISHED
9 March 2023

Abstract

Mesoscale eddies play an important role in the transport of heat, carbon, and nutrients in the Southern Ocean. Previous studies have documented an increasing intensity of the Southern Ocean eddy field during recent decades; however, it remains unclear whether the mesoscale eddies with different lifetimes have different temporal variations. Using satellite altimeter observations from 1993 to 2020, we found that the increasing trend in the intensity of eddies is dominated by long-lived eddies (with lifetimes $\geqslant$ 90 d), whose amplitude has increased at a rate of ~2.8% per decade; the increase is concentrated downstream of topography. In contrast, short-lived eddies (with lifetimes $<$ 90 d) do not appear to have a significant trend in their amplitudes since the early 1990s. An energy conversion analysis indicates that the increased baroclinic instabilities of the mean flows associated with topography are responsible for the amplitude increase of the long-lived eddies. This study highlights the need for a better understanding of the changes in mesoscale eddies owing to their importance in the transport of heat, carbon, and nutrients.

1. Introduction

The Southern Ocean (SO) is a key component of the global climate system that has experienced pronounced subsurface warming alongside westerly wind strengthening in recent decades (Böning *et al* 2008, Waugh *et al* 2013, Shi *et al* 2021). Mesoscale eddies play key roles in the SO by redistributing the Antarctic circumpolar circulation (ACC) and influencing the transport of heat, carbon, and nutrients (Screen *et al* 2009, Chelton *et al* 2011, Keppler and Landschützer 2019, Friedrichs *et al* 2022, Morrison *et al* 2022). Primarily due to anthropogenic ocean warming and secondarily owing to wind stress strengthening, the ACC has been observed and modeled to undergo robust zonal acceleration (Shi *et al* 2020, 2021). The response of the ACC and the upper cell of the circumpolar meridional overturning circulation to changes in wind stress were previously explained by two hypotheses: 'eddy saturation' and 'eddy compensation' (Straub 1993, Hallberg and Gnanadesikan 2001, 2006, Hogg *et al* 2008, Hogg 2010, Viebahn and Eden 2010).

Due to the dynamic importance of mesoscale eddies, much attention has been paid to changes in the eddy kinetic energy (EKE) in the SO since the advent of satellite altimetry (Fu *et al* 2010). For example, a robust increase in the EKE field has been observed since 1993, with larger trends in the Pacific and Indian sectors (Meredith and Hogg 2006, Hogg *et al* 2015, Menna *et al* 2020). Following Hogg *et al* (2015), Martínez-Moreno *et al* (2019, 2022) decomposed the eddy field into mesoscale eddies and residual components and demonstrated that the increasing trend of EKE is mainly impacted by mesoscale eddies. Moreover, the EKE field shows a more significant increase of 2%–5% per decade in the eddy-rich regions. In comparison, Zhang *et al* (2021) pointed

out that EKE increases significantly only downstream of the Campbell Plateau rather than in other regions along the ACC. The causes for the long-term changes in the EKE are thought to be due to a strengthening of the wind stress with delays of 1–4 years (Hogg *et al* 2015, Menna *et al* 2020). The high-resolution model also showed an increase in EKE that peaks 2–3 years after a positive peak in the Southern Annular Mode (SAM) index (Screen *et al* 2009). Besides external wind-forced changes in the EKE, high-resolution modeling has suggested that the eddy field also exhibited a chaotic internal nature, which may mask wind-driven changes (Meredith 2016, Patara *et al* 2016, Hogg *et al* 2022). Another important feature is the spatial pattern of the EKE field, which is collocated with major topography and is primarily determined by the instability of the mean flow (Graham *et al* 2012, Barthel *et al* 2017, Chapman 2017, Youngs *et al* 2017, Cai *et al* 2022). Model experiments showed that the EKE depends on the shape and height of the topography as well as on the baroclinicity of the jet, but it is not very sensitive to increased wind stress (Barthel *et al* 2017, Cai *et al* 2022). The nonlinear evolution of the instability leads to an inverse cascade of energy and likely determines the eddy properties (Pedlosky 1987, Scott and Wang 2005, Venaille *et al* 2011); however, the long-term changes in barotropic and baroclinic instabilities and their connections with eddy variations in the SO remain unexplored.

Previous studies have mainly focused on the EKE field, which includes features like waves, meanders, and eddies of multiple scales; however, it is still unclear whether the mesoscale eddies with different lifetimes temporally differ in their variations. This study investigates how mesoscale eddies with different lifetimes respond to the SO changes and the possible physical processes responsible for those changes. To answer these questions, we explore the long-term trends in mesoscale eddies identified and tracked from satellite altimeter records from 1993 to 2020; we find that the increasing intensity trends are dominated by eddies with longer lifetimes, with the short-lived eddies only contributing slight changes. The mechanism behind this is illustrated by the increasing trends in energy conversion due to baroclinic instability. The remainder of this paper is organized as follows: section 2 introduces the data and methods, the results are described in section 3, and the discussion and conclusions are outlined in section 4.

2. Data and methods

2.1. Satellite altimeter and sea surface temperature products

The daily surface height (SSH) and derived surface geostrophic speeds have a horizontal resolution of $1/4^\circ$ from 1993 to 2020. Mesoscale eddies with coherent structures are identified and tracked based on the SSH after removing the large-scale variability, and eddy trajectory atlas products (META3.2 DT) are developed (Mason *et al* 2014, Pegliasco *et al* 2022). In the atlas, the eddy amplitude ($\mathrm{Eddy}_{\mathrm{amp}}$) is defined as the magnitude of the difference between the extremum of SSH within the eddy and the SSH around the eddy edge, which exhibits a linear relationship with the surface geostrophic speed; the eddy length scale is equal to the diameter of an eddy that has the area of the coherent structure, $L_e = 2\sqrt{\mathrm{area}/\pi}$. Details on the eddy characteristics are described in Pegliasco *et al* (2022).

Mesoscale eddies with lifetimes shorter than 10 d are not considered herein since the resolvable temporal scale of the product is around 10 d (Pujol *et al* 2016, Chen and Han 2019). To reduce noise in the data, eddies with amplitudes smaller than 2 cm are also discarded. The present work divides the eddies into two groups based on their lifetimes. One group consists of short-lived eddies with lifetimes shorter than 90 d but longer than 10 d; the other group consists of long-lived eddies with lifetimes equal to or longer than 90 d. The median lifetime of eddies is around three months, among which the short-lived and long-lived eddies account for 52% and 45% of the totals, respectively (table S1). Our review of the results indicates that the conclusions of this analysis are not very sensitive to how the short- and long-lived eddies are partitioned (figures 1 and S2, S3).

The National Oceanic and Atmospheric Administration Daily Optimum Interpolation Sea Surface Temperature (OISST) incorporates observations from different platforms into a regular global grid (Huang *et al* 2021). The OISST v2.1 product has a horizontal resolution of $1/4^\circ$ and is available from September 1981 to the present. We analyze the period of overlap with the eddy trajectory atlas from January 1993 to December 2020.

2.2. Energy conversion

Energy equations provide a quantitative description of the energy exchange between eddies and the mean flow (Cronin and Watts 1996, Eden and Böning 2002, Kang and Curchitser 2015). Through instability processes, eddies can extract energy from the mean flow, where a barotropic conversion process (BT) occurs from the mean kinetic energy (MKE) to the EKE, and a baroclinic conversion process (BC) occurs from the mean potential energy (MPE) to the eddy potential energy (EPE). Due to the lack of long-term salinity observations, following Cronin and Watts (1996), the SST variability is used to represent the approximate density variability in the surface layer, using $\rho = \rho_0 (1 - \varphi T)$. The temperature trend at the surface shows a pattern similar to those in the upper SO (figure S1), which suggests that the SST is roughly representative of the long-term changes in the upper

ocean temperatures. Thus, we calculate the BT and BC in the surface layer as follows:

$$\mathrm{BT} = -\rho_0 \left[\overline{u'^2} \frac{\partial \bar{u}}{\partial x} + \overline{v'^2} \frac{\partial \bar{v}}{\partial y} + \overline{u'v'} \left(\frac{\partial \bar{v}}{\partial x} + \frac{\partial \bar{u}}{\partial y} \right) \right], \tag{1}$$

and

$$\begin{aligned} \mathrm{BC} &= -\frac{g^2}{\overline{N^2}\rho_0} \left(\overline{u'\rho'} \frac{\partial \bar{\rho}}{\partial x} + \overline{v'\rho'} \frac{\partial \bar{\rho}}{\partial y} \right) \\ &= -\frac{\rho_0 \alpha g}{\frac{\partial \bar{T}}{\partial z}} \left(\overline{u'T'} \frac{\partial \bar{T}}{\partial x} + \overline{v'T'} \frac{\partial \bar{T}}{\partial y} \right), \end{aligned} \tag{2}$$

where $\bar{u}$, $\bar{v}$, $\bar{\rho}$, and $\bar{T}$ are the time-mean zonal and meridional velocity, seawater density, and temperature from 1993 to 2020, respectively; u', v', ρ', and T' are the time-varying zonal and meridional velocity, seawater density, and temperature, respectively. In the equations, g, ρ_0, φ, and N^2 are an acceleration of gravity, a constant density of 1025 kg m^{-3}, thermal expansion, and the buoyancy frequency, respectively. The mesoscale eddies emerge from the barotropic instability of strongly horizontal velocity shear or are generated by baroclinic instability from the collapsing of horizontal density gradients. The BT and BC are direct sources of eddy growth, with positive values indicating eddy formation.

3. Results

3.1. Changes in eddies with different lifetimes

Here, we begin to explore changes in the amplitude ($\mathrm{Eddy_{amp}}$) and number ($\mathrm{Eddy_{num}}$) of the eddies with different lifetimes over the region between 45°S and 65°S, which roughly covers the ACC path and its surroundings (figures 1 and S2). Figure 1(a) shows that all eddies have increased amplitudes since the early 1990s, with the increase being much more significant for the eddies with lifetimes longer than 90 d. The amplitude increase of the long-lived eddies has reached a rate of 0.26 ± 0.06 cm or $2.8 \pm 0.6\%$ per decade (figure 1(c)), which is consistent with trends in the EKE (Martínez-Moreno *et al* 2021), while the amplitude of the short-lived eddies does not appear to have had a significant change during the past a few decades (figure 1(c)). In addition, the variability of the eddies with lifetimes longer than 10 d is collocated with that of the long-lived eddies (figure 1(c)), indicating that the long-lived eddies are largely responsible for the changes and variations in the eddy amplitude in the SO. There is also an increasing trend in the number of eddies that are dominated by long-lived eddies (figures 1(b) and (d)). These may be a consequence of more long-lived eddies being formed or small eddies merging into larger ones through eddy–eddy interaction (the transfer of energy from small to large scales) (Grooms 2015).

Following Samelson *et al* (2014) and Pegliasco *et al* (2015), the evolution of a mesoscale eddy is divided into three stages, with 0%–15% of its lifetime as the growing phase, 15%–85% as the mature phase, and 85%–100% as the decaying phase. Because the development of eddies is sourced from the energy of the mean flow, the changes in the amplitude and number of eddies are further explored during their growing phase (figures 1(e) and (f)). The long-lived eddies in the growing phase strengthened at a rate of 0.26 ± 0.2 cm or $3.2\% \pm 2.7\%$ per decade, while the short-lived eddies show small changes in their amplitudes (figure 1(e)). The number of long-lived eddies in the growing phase has increased slightly with a large standard error and is barely significant at the 95% confidence level (figure 1(f)); by comparison, the number of short-lived eddies does not appear to exhibit a significant change. This analysis reveals that much larger increases in the amplitude of the long-lived eddies than in the short-lived eddies may be induced by more energy extraction in the growing period.

3.2. Spatial features of the trends

The spatial distribution of eddies suggests that eddy generation in the SO is not uniform but is centralized around five hotspots. Considering figures 2(a)–(c), the five hot spots of eddies are all located downstream of major topographic features along the ACC, which is consistent with the findings of previous studies (Zajaczkovski 2017). While the five hotspots of the long-lived eddies are collocated with those of the short-lived eddies, the long-lived eddies are distributed more widely due to their ability to propagate farther away (figures 2(b) and (c)). Figures 2(d) and (e) show that the trends in the amplitudes of the eddies are highly heterogeneous along the ACC, with larger trends concentrated in the eddy-rich area downstream of the topography. The increasing trend in the amplitude of the eddies is dominated by the long-lived eddies, whose amplitude has increased at a rate of up to 0.3 cm per decade. In contrast, the short-lived eddies appear to have a much weaker increasing trend in their amplitudes. These spatial variations may reflect the impacts of local wind stress or interactions between the ACC and local topography (Thompson and Garabato 2014, Rintoul 2018).

To further explore changes in the amplitudes of short-lived and long-lived eddies in the eddy-rich regions (figure S4), we divide the main ACC path into five subregions, each roughly covering one hotspot of eddies (figure 2(b)). The amplitudes of long-lived eddies have increased significantly above the 95% confidence level in the R2–R5, with the largest trends in the R2 at a rate of ~0.3 cm or 3.5% per decade, while the amplitude of long-lived eddies appears to decrease slightly in the R1 at a rate of $0.9 \pm 0.6\%$

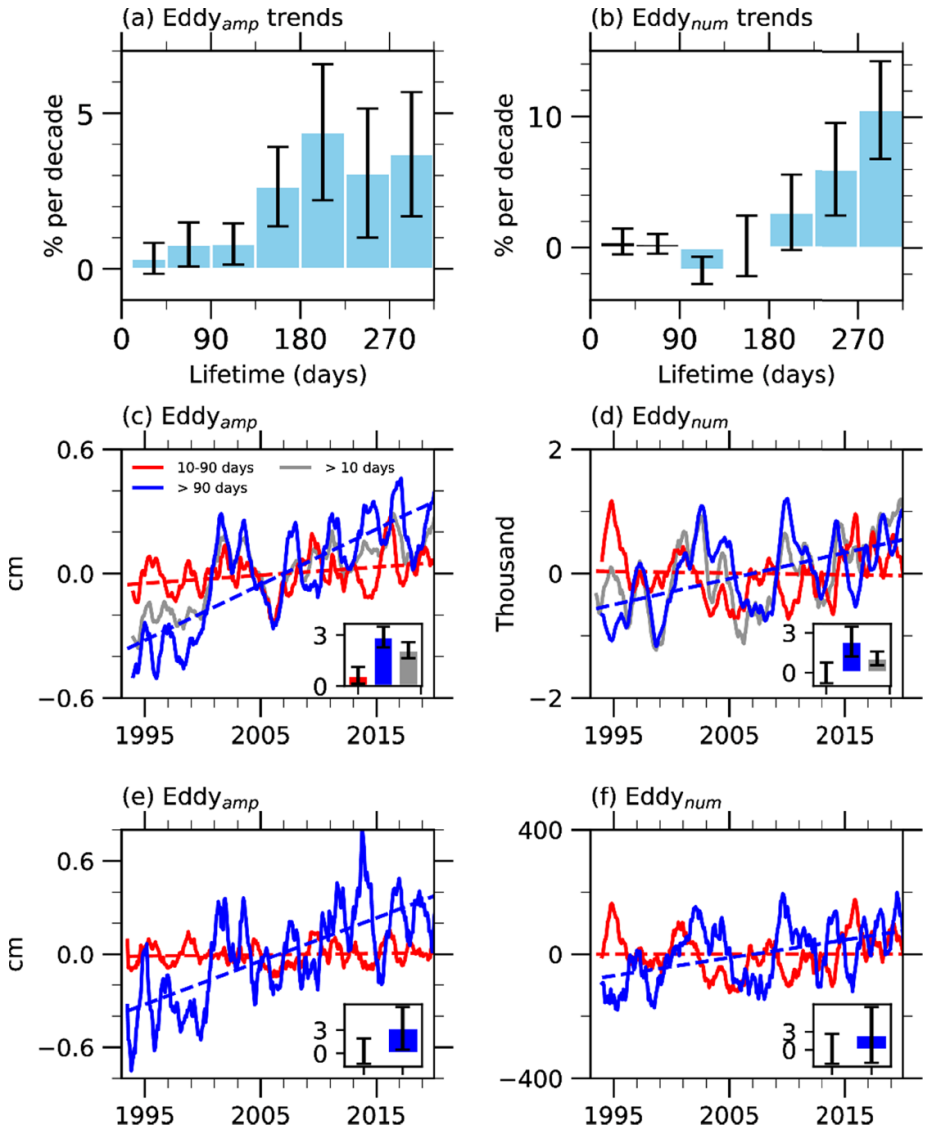

Figure 1. Trends in the (a) amplitude (Eddy$_{amp}$) and (b) number (Eddy$_{num}$) of eddies with different lifetimes in 45-day bins. The error bars denote the standard deviations of the annual mean values. Time series of the (c) Eddy$_{amp}$ and (d) Eddy$_{num}$ anomalies of the short-lived eddies (with lifetimes between 10 and 90 d), long-lived eddies (lifetimes $\geqslant$ 90 d), and all eddies (lifetimes $>$ 10 d) in the SO (45°S − 65°S). The Eddy$_{amp}$ and Eddy$_{num}$ trends in the long-lived eddies are 0.26 $\pm$ 0.06 cm and 391 $\pm$ 188 per decade with p-value $<$ 0.001 respectively. Time series of (e) Eddy$_{amp}$ and (f) Eddy$_{num}$ anomalies of short-lived and long-lived eddies during their growing period (the first 15% of their lifetimes). The Eddy$_{amp}$ and Eddy$_{num}$ trends in the long-lived eddies are 0.26 $\pm$ 0.2 cm and 59 $\pm$ 110 per decade with p-value $<$ 0.001 respectively. In (c)–(f), the solid curves are 12 month moving averages, and dashed lines are the trends above the 95% confidence level; the insets in the lower right of each panel show the corresponding trends in units of percent per decade.

per decade. Note that the zonal flow and BC in the R1 have not strengthened as much as in other subregions, which indicates that the amplitude of eddies in this region may not increase as much as in other subregions. In contrast, the amplitudes of short-lived eddies show no robust trends in the R1, R2, R3, and R5, barely significantly above the 95% confidence level, but they show a weak increasing trend in the R4 at a rate of ∼0.1 cm or 1.7% per decade. The contrasting trends in the eddy amplitudes in the five hotspots indicate the importance of local dynamics, such as local wind stresses and interactions between the mean flow and local topography (Thompson and Garabato 2014, Rintoul 2018).

3.3. Mechanism for the trends in the eddy amplitudes

The above analysis finds that the mesoscale eddies have increasing amplitude trends in the SO, with the trend being more significant for the long-lived eddies in several hotspots along the ACC (figure 2(e)). Around the five eddy-rich regions along the ACC jet, there appears to be positive mean energy conversion from the MKE to the EKE (BT) due to barotropic instabilities of the mean flow (figure S5), which is consistent with the distribution of the energetic eddy field. The BT is small near the Southwest Indian Ridge (SWIR) but large near the Kerguelen Plateau (KP), Maquarie Ridge (MR), Pacific Antarctic Ridge

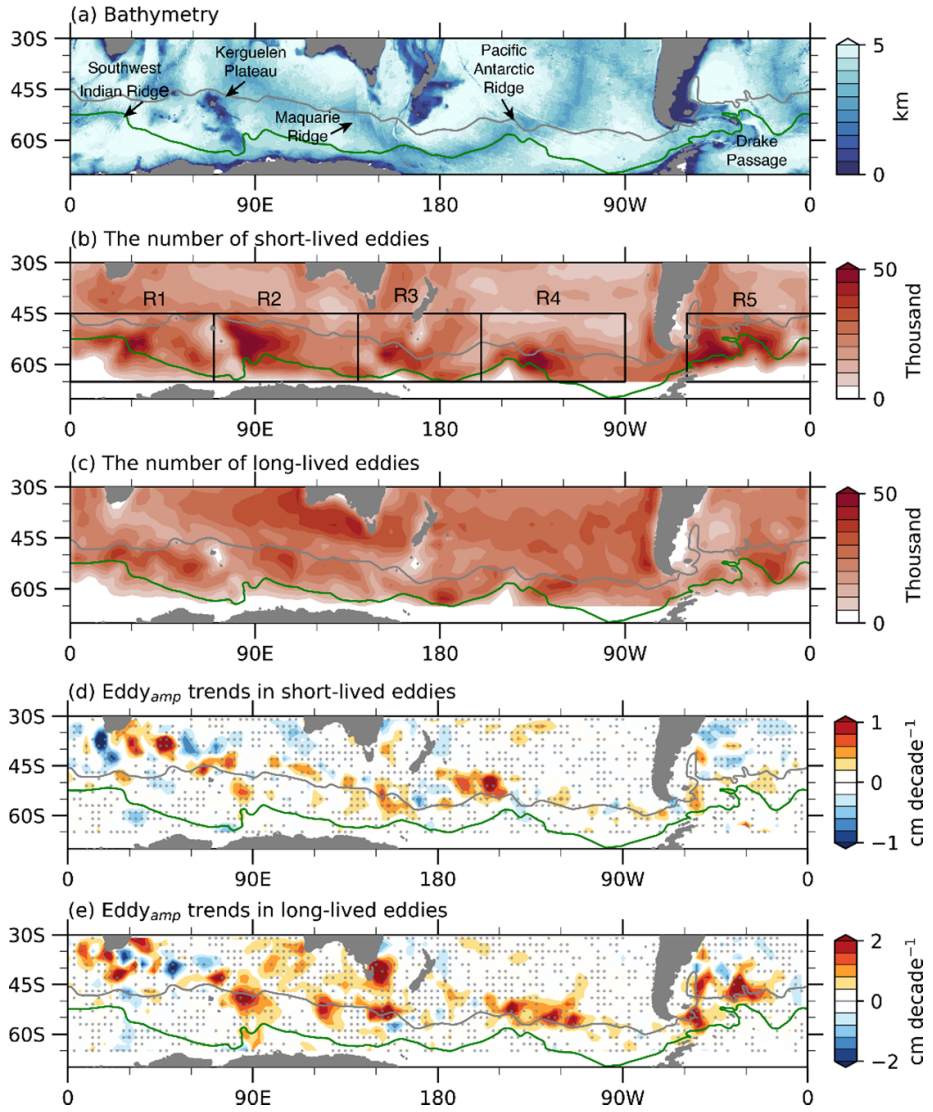

Figure 2. (a) The bathymetry, the number of (b) short-lived and (c) long-lived eddies, and the amplitude trend of (d) short-lived and (e) long-lived eddies in 6° × 4° bins. The gray stippling indicates that the trends are statistically significant at the 95% confidence level. The curves indicate the Subantarctic Front (gray contour) and Southern ACC Front (green contour), respectively (Orsi *et al* 1995). The five eddy-rich regions (R1: 0 − 70°E, R2: 70 − 140°E, R3: 140 − 200°E, R4: 200 − 270°E, and R5: 300 − 360°E) are defined from west to east meridionally between 45°S and 65°S to cover the main ACC path. The five major topographic features are the Southwest Indian Ridge (SWIR), Kerguelen Plateau (KP), Maquarie Ridge (MR), Pacific Antarctic Ridge (PAR), and Drake Passage (DP).

(PAR), and Drake Passage (DP), with the maximum reaching $\sim 1-5\times10^{-4}$ Wm^{-2}. The energy conversion from the MPE to the EPE (BC) due to baroclinic instabilities is also centralized around the eddy-rich regions, and its value is much larger than that of the BT, reaching $\sim 5-10\times10^{-4}$ Wm^{-2}, which indicates more energy is being released from the baroclinic instabilities. Moreover, the locations of the elevated eddy energy and the BC coincide with the bottom topography but not with those of strengthened winds, which implies the primary role of topography in shaping eddy activity patterns along the ACC (e.g. Graham *et al* 2012, Thompson and Sallée 2012, Barthel *et al* 2017, Cai *et al* 2022).

Both the BT and BC have increased significantly around the five eddy-rich regions since the early 1990s, with the trend for the latter being much larger than that for the former (figures 3(a) and (b)). The pattern of the BC trend agrees well with the topography, with a maximum of $\sim 3\times10^{-4}$ Wm^{-2} per decade (figure 3(b)). The long-term change in the BC is correlated well with a surface-accelerated zonal geostrophic velocity with a correlation coefficient of 0.64 (figure 3(c)). The close link of the BC to the topography indicates that the BC is sourced from interactions between the accelerated mean flow and topography. Meanwhile, the amplitude change of the long-lived eddies is highly significantly correlated with the change in the BC, with a correlation coefficient of 0.79 and a lag of three months, suggesting that baroclinic instability is the main process providing the energy for increasing the intensity of the eddies. A cross wavelet transform (Grinsted *et al* 2004) of the eddy amplitude and the BC time series

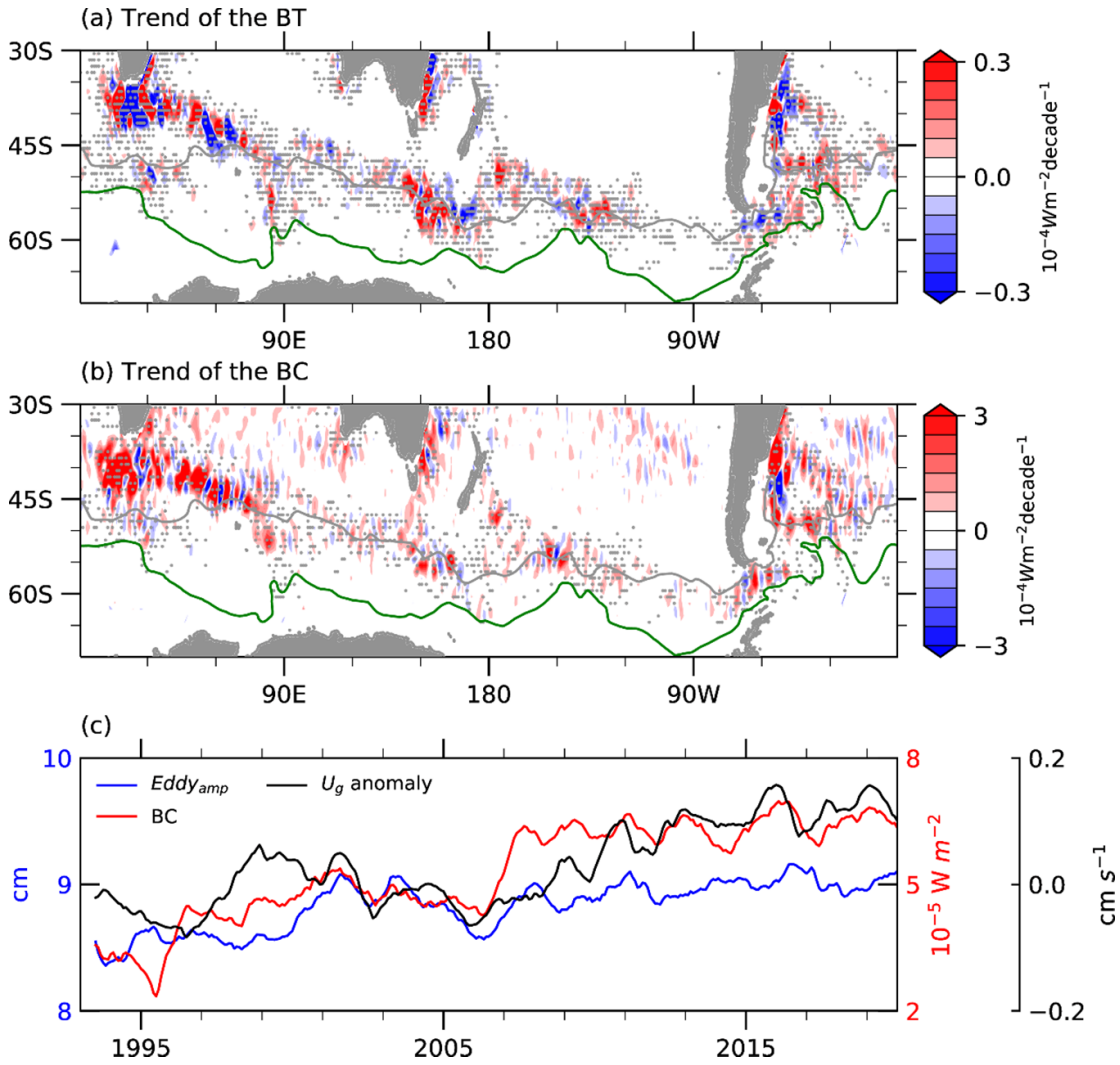

Figure 3. Trends in the (a) barotropic and (b) baroclinic energy conversion in the surface layer. The gray stippling indicates that the trends are statistically significant at the 95% confidence level. (c) Time series of the amplitude of the long-lived eddies (blue curve), the BC in the surface layer (red curve), and the surface zonal geostrophic velocity U_g anomaly (black curve) averaged between 45°N and 65°N (Pearson correlation coefficient r between the Eddy_{amp} and the BC is 0.79 with p-value < 0.001). Reproduced from Guo Y CC BY 4.0.

also shows that most of the power is concentrated within the band of 1–4 years (figure S7), suggesting a consistent phase relationship between them. But why these long-lived eddies? According to Scott and Wang (2005) and Tulloch *et al* (2011), the most unstable scale of instabilities has a wavelength a few times larger than the deformation radius, which is ∼100 km along the ACC path, as estimated from linear instability theory, $2\pi L_d$, where L_d is the first Rossby radius of deformation (figure S6). In other words, the maximum perturbation energy can be expected at a scale of ∼100 km. By scale estimation, the mean length scales of long-lived eddies when they are detected for the first time are about 90–100 km, which corresponds well to the most unstable scale, while the length scales of short-lived eddies are much smaller. Moreover, we further calculate the detrended time series of the length scale of the long-lived eddies and the BC (figure S8). The length scale change of the long-lived eddies is highly correlated with the change in the BC, with a correlation coefficient of 0.53, indicating that the long-lived eddies at the unstable scales co-vary with the BC and the BC provides the main energy for the increasing intensity of the long-lived eddies. Therefore, increased baroclinic instabilities support amplitude increases of the long-lived eddies whose scale is near that of the energy source in the SO.

4. Conclusions and discussion

Our findings identified long-lived eddies that have dominated the increasing eddy intensity trend based on satellite altimeter observations from 1993 to 2020 in the SO; the increased baroclinic instabilities responsible for these long-term changes along the ACC path (between 45°S and 65°S) were also identified. Moreover, there are substantial longitudinal variations in the eddy amplitude trends, with a larger increase downstream of the major topography. As

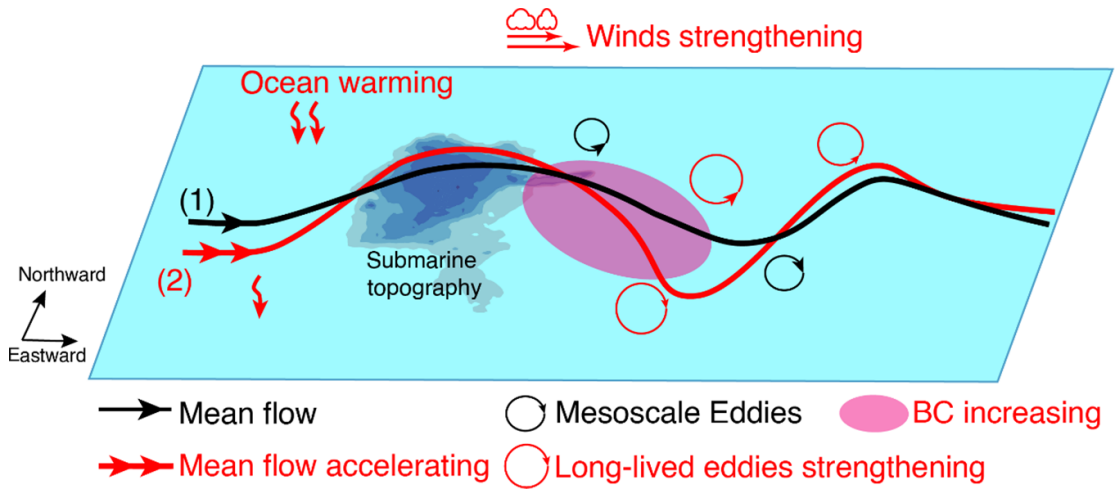

Figure 4. Schematic diagram of possible physical processes underlying the eddy amplitude increase along the ACC path. Red curves and text indicate the changes from a reference state (black curves) in response to the SO warming and an increase in wind stress. (1) The ACC interacts with topography, which shapes the features of the elevated eddy field downstream of the topography. (2) In response to the SO warming and the westerly wind strengthening, the ACC undergoes zonal acceleration, the meander curvature increases, and meridional density gradients become greater. As a consequence, the BC of the mean flow significantly increases there, driving the amplitude increase of eddies with longer lifetimes whose scales are near the most unstable scale.

summarized in the schematic diagram in figure 4, the ACC jet is largely zonal upstream of the topography where the eddy energy is relatively low. When the jet encounters the major topography, the water columns are squashed/stretched and move equatorward/poleward, leading to a meander curvature and an unstable flow, which shapes the features of the elevated eddy field downstream of the topography (Barthel *et al* 2017, Rintoul 2018, Cai *et al* 2022). Because the SO experienced pronounced warming in recent decades, more (less) warming north (south) of the ACC caused greater isopycnal tilting and robust zonal acceleration (Shi *et al* 2021). At the same time, the SAM experienced an increasing trend, showing us that the zonal winds have intensified. The strengthening westerly winds contributed to steepening the isopycnal slopes, while the increased meander curvature adjusted to balance the increased zonal transports (Thompson and Garabato 2014), which resulted in enhanced eddy activities. As a consequence, the BC of the mean flow significantly increased, which is more favorable for releasing available potential energy. These increased instabilities provided favorable conditions for the generation of more energetic eddies with longer lifetimes whose scales are ~90 km.

Despite the significant amplitude increases of long-lived eddies, as shown herein, the amplitudes of short-lived eddies have changed little. Given short-lived eddies' lifetimes (defined here as between 10 and 90 d), these results may partly reflect the stochastic, chaotic nature of these eddies (Hogg *et al* 2022) and partly represent changes in eddies with relatively long lifetimes. In addition, much of the existing research has indicated that the ocean is saturated with nonlinear eddies that merge, split, and couple with one another (Grooms 2015). We found that the number of long-lived eddies also slightly increased in recent years, but the trend in the number of short-lived eddies was not significant. It seems that more long-lived eddies develop partly from eddy–eddy interaction. Note that we only consider the tracked eddies with lifetimes larger than 10 d and amplitudes larger than 2 cm. Martínez-Moreno *et al* (2019) found a decreasing trend in the number of eddies because they identified transient eddies using different algorithms and a larger area between 30°S – 60°S. In the coming decades, the future SO is projected to experience pronounced subsurface warming alongside westerly wind strengthening, which would have greater impacts on the ACC, the BC and the eddy fields. However, the projected change in the SO is still an open question due to the change in the El Niño–Southern Oscillation (ENSO). Wang *et al* (2022) showed a greater projected increase in ENSO amplitude weakens high-latitude westerly poleward intensification and slows future SO warming.

In summary, the present study indicates that long-lived eddies strengthened at a quicker rate in response to climate change (ocean warming and wind intensification) in the SO, which highlights the need for further understanding the changes in eddies on separate scales instead of considering them together. Mesoscale processes make a large contribution to the poleward transport of heat, carbon, and nutrients (Screen *et al* 2009, Guo *et al* 2022, Morrison *et al* 2022). An increasing trend in surface eddy heat flux has been observed associated with increasing eddy energetics. Due to their ability to trap large water mass and induce large velocity anomalies, long-lived eddies may play a more important role in transporting heat, carbon, and nutrients in the future (Screen *et al* 2009, Chelton *et al* 2011, Keppler and Landschützer 2019).

Data availability statements

All data used in this study are publicly accessible from these websites: the satellite altimeter products: https://doi.org/10.48670/moi-00148; the eddy trajectory atlas: https://doi.org/10.24400/527896/a01-2022.005.220209; the SST products OISST v.2.1: www.ncei.noaa.gov/products/optimum-interpolation-sst. The trend analysis uses xarrayMannKendall (https://doi.org/10.5281/zenodo.4458776).

All data that support the findings of this study are included within the article (and any supplementary files).

Acknowledgments

This work was supported by the National Natural Science Foundation of China (No. 42230405, 41976006 and 42006029), the Southern Marine Science and Engineering Guangdong Laboratory (Zhuhai) (Grant SML2021SP302), the Program of Marine Economy Development Special Fund (Six Marine Industries) under Department of Natural Resources of Guangdong Province, (Project No. GDNRC [2022]18), the National Key R&D Program of China (Grant No. 2019YFC1509102).

Conflict of interest

None declared.

ORCID iD

Fei Shi https://orcid.org/0000-0001-6362-7386

References

Barthel A, Hogg A M C, Waterman S and Keating S 2017 Jet-topography interactions affect energy pathways to the deep Southern Ocean *J. Phys. Oceanogr.* **47** 1799–816

Böning C W, Dispert A, Visbeck M, Rintoul S R and Schwarzkopf F U 2008 The response of the Antarctic Circumpolar Current to recent climate change *Nat. Geosci.* **1** 864–9

Cai Y, Chen D, Mazloff M R, Lian T and Liu X 2022 Topographic modulation of the wind stress impact on eddy activity in the Southern Ocean *Geophys. Res. Lett.* **49** e2022GL097859

Chapman C C 2017 New perspectives on frontal variability in the Southern Ocean *J. Phys. Oceanogr.* **47** 1151–68

Chelton D B, Schlax M G and Samelson R M 2011 Global observations of nonlinear mesoscale eddies *Prog. Oceanogr.* **91** 167–216

Chen G and Han G 2019 Contrasting short-lived with long-lived mesoscale eddies in the global ocean *J. Geophys. Res. Ocean* **124** 3149–67

Cronin M and Watts D R 1996 Eddy–mean flow interaction in the Gulf Stream at 68°W. Part i: eddy energetics *J. Phys. Oceanogr.* **26** 2107–31

Eden C and Böning C 2002 Sources of eddy kinetic energy in the Labrador Sea *J. Phys. Oceanogr.* **32** 3346–63

Friedrichs D M *et al* 2022 Observations of submesoscale eddy-driven heat transport at an ice shelf calving front *Commun. Earth Environ.* **3** 1–9

Fu L L, Chelton D B, Le Traon P Y and Morrow R 2010 Eddy dynamics from satellite altimetry *Oceanography* **23** 14–25

Graham R M, de Boer A M, Heywood K J, Chapman M R and Stevens D P 2012 Southern Ocean fronts: controlled by wind or topography? *J. Geophys. Res. Ocean* **117** 20

Grinsted A, Moore J C and Jevrejeva S 2004 Application of the cross wavelet transform and wavelet coherence to geophysical time series *Nonlinear Process. Geophys.* **11** 561–6

Grooms I 2015 A computational study of turbulent kinetic energy transport in barotropic turbulence on the f-plane *Phys. Fluids* **27** 101701

Guo Y, Bachman S, Bryan F and Bishop S 2022 Increasing trends in oceanic surface poleward eddy heat flux observed over the past three decades *Geophys. Res. Lett.* **49** e2022GL099362

Hallberg R and Gnanadesikan A 2001 An exploration of the role of transient eddies in determining the transport of a zonally reentrant current *J. Phys. Oceanogr.* **31** 3312–30

Hallberg R and Gnanadesikan A 2006 The role of eddies in determining the structure and response of the wind-driven Southern hemisphere overturning: results from the modeling eddies in the Southern Ocean (MESO) project *J. Phys. Oceanogr.* **36** 2232–52

Hogg A M C 2010 An Antarctic Circumpolar Current driven by surface buoyancy forcing *Geophys. Res. Lett.* **37**

Hogg A M C, Meredith M P, Blundel J R and Wilson C 2008 Eddy heat flux in the Southern Ocean: response to variable wind forcing *J. Clim.* **21** 608–20

Hogg A M C, Meredith M P, Chambers D P, Abrahamsen E P, Hughes C W and Morrison A K 2015 Recent trends in the Southern Ocean eddy field *J. Geophys. Res. Ocean* **120** 257–67

Hogg A M C, Penduff T, Close S E, Dewar W K, Constantinou N C and Martínez-Moreno J 2022 Circumpolar variations in the chaotic nature of Southern Ocean eddy dynamics *J. Geophys. Res. Ocean* **127** e2022JC018440

Huang B, Liu C, Banzon V, Freeman E, Graham G, Hankins B, Smith T and Zhang H M 2021 Improvements of the daily optimum interpolation sea surface temperature (DOISST) version 2.1 *J. Clim.* **34** 715–36

Kang D and Curchitser E N 2015 Energetics of eddy-mean flow interactions in the Gulf Stream region *J. Phys. Oceanogr.* **45** 1103–20

Keppler L and Landschützer P 2019 Regional wind variability modulates the Southern Ocean carbon sink *Sci. Rep.* **9**

Martínez-Moreno J, Hogg A M C and England M H 2022 Climatology, seasonality, and trends of spatially coherent ocean eddies *J. Geophys. Res. Ocean* **127** e2021JC017453

Martínez-Moreno J, Hogg A M C, Kiss A E, Constantinou N C and Morrison A K 2019 Kinetic energy of eddy-like features from sea surface altimetry *J. Adv. Model. Earth Syst.* **11** 3090–105

Martínez-Moreno J, Hogg A M, England M H, Constantinou N C, Kiss A E and Morrison A K 2021 Global changes in oceanic mesoscale currents over the satellite altimetry record *Nat. Clim. Change* **11** 397–403

Mason E, Pascual A and McWilliams J C 2014 A new sea surface height-based code for oceanic mesoscale eddy tracking *J. Atmos. Ocean. Technol.* **31** 1181–8

Menna M, Cotroneo Y, Falco P, Zambianchi E, di Lemma R, Poulain P-M, Fusco G and Budillon G 2020 Response of the Pacific sector of the Southern Ocean to wind stress variability from 1995 to 2017 *J. Geophys. Res. Ocean* **125** 1–18

Meredith M P 2016 Understanding the structure of changes in the Southern Ocean eddy field *Geophys. Res. Lett.* **43** 5829–32

Meredith M P and Hogg A M 2006 Circumpolar response of Southern Ocean eddy activity to a change in the southern annular mode *Geophys. Res. Lett.* **33** L16608

Morrison A K, Waugh D W, Hogg A M C, Jones D C and Abernathey R P 2022 Ventilation of the Southern Ocean Pycnocline *Ann. Rev. Mar. Sci.* **14** 405–30

Orsi A H, Whitworth T and Nowlin W D 1995 On the meridional extent and fronts of the Antarctic Circumpolar Current *Deep. Res.* I **42** 641–73

Patara L, Böning C W and Biastoch A 2016 Variability and trends in Southern Ocean eddy activity in 1/12° ocean model simulations *Geophys. Res. Lett.* **43** 4517–23

Pedlosky J 1987 *Geophysical Fluid Dynamics* (New York: Springer) (https://doi.org/10.1007/978-1-4612-4650-3_2)

Pegliasco C, Chaigneau A and Morrow R 2015 Main eddy vertical structures observed in the four major Eastern boundary upwelling systems *J. Geophys. Res. Ocean* **120** 6008–33

Pegliasco C, Delepoulle A, Mason E, Morrow R, Faugère Y and Dibarboure G 2022 META3.1exp: a new global mesoscale eddy trajectory atlas derived from altimetry *Earth Syst. Sci. Data* **14** 1087–107

Pujol M I, Faugère Y, Taburet G, Dupuy S, Pelloquin C, Ablain M and Picot N 2016 DUACS DT2014: the new multi-mission altimeter data set reprocessed over 20 years *Ocean Sci.* **12** 1067–90

Rintoul S R 2018 The global influence of localized dynamics in the Southern Ocean *Nature* **558** 209–18

Samelson R M, Schlax M G and Chelton D B 2014 Randomness, symmetry, and scaling of mesoscale eddy life cycles *J. Phys. Oceanogr.* **44** 1012–29

Scott R B and Wang F 2005 Direct evidence of an oceanic inverse kinetic energy cascade from satellite altimetry *J. Phys. Oceanogr.* **35** 1650–66

Screen J A, Gillet N P, Stevens D P, Marshall G J and Roscoe H K 2009 The role of eddies in the Southern Ocean temperature response to the southern annular mode *J. Clim.* **22** 806–18

Shi J-R, Talley L D, Xie S-P, Liu W and Gille S T 2020 Effects of buoyancy and wind forcing on Southern Ocean climate change *J. Clim.* **33** 10003–20

Shi J-R, Talley L D, Xie S-P, Peng Q and Liu W 2021 Ocean warming and accelerating Southern Ocean zonal flow *Nat. Clim. Change* **11** 1090–7

Straub D N 1993 On the transport and angular momentum balance of channel models of the Antarctic Circumpolar Current *J. Phys. Oceanogr.* **23** 776–82

Thompson A F and Garabato A C N 2014 Equilibration of the Antarctic Circumpolar Current by standing meanders *J. Phys. Oceanogr.* **44** 1811–28

Thompson A F and Sallée J B 2012 Jets and topography: jet transitions and the impact on transport in the Antarctic Circumpolar Current *J. Phys. Oceanogr.* **42** 956–72

Tulloch R, Marshall J, Hill C and Smith K S 2011 Scales, growth rates, and spectral fluxes of baroclinic instability in the ocean *J. Phys. Oceanogr.* **41** 1057–76

Venaille A, Vallis G K and Smith K S 2011 Baroclinic turbulence in the ocean: analysis with primitive equation and quasigeostrophic simulations *J. Phys. Oceanogr.* **41** 1605–23

Viebahn J and Eden C 2010 Towards the impact of eddies on the response of the Southern Ocean to climate change *Ocean Model.* **34** 150–65

Wang G, Cai W, Santoso A, Wu L, Fyfe J C, Yeh S W, Ng B, Yang K and McPhaden M J 2022 Future Southern Ocean warming linked to projected ENSO variability *Nat. Clim. Change* **12** 649–54

Waugh D W, Primeau F, DeVries T and Holzer M 2013 Recent changes in the ventilation of the Southern Oceans *Science* **339** 568–70

Youngs M K, Thompson A F, Lazar A and Richards K J 2017 ACC meanders, energy transfer, and mixed barotropic-baroclinic instability *J. Phys. Oceanogr.* **47** 1291–305

Zajaczkovski U 2017 *A Study of the Southern Ocean: Mean State, Eddy Genesis & Demise, and Energy Pathways* (San Diego: University of California)

Zhang Y, Chambers D and Liang X 2021 Regional trends in Southern Ocean eddy kinetic energy *J. Geophys. Res. Ocean* **126**